International Journal of Technology 13(5) 1139-1148 (2022)
Received April 2022 / Revised August 2022 / Accepted August 2022

International Journal of Technology

http://ijtech.eng.ui.ac.id

A Novel Lattice Structure for Enhanced Crush Energy Absorption

Chang Yuan Seek[1], Chee Kuang Kok[2*], Chong Hooi Lim[3], Kia Wai Liew[2]

[1]*STMicroelectronics Sdn. Bhd., Kawasan Perindustrian Tanjung Agas, 84007 Muar, Johor, Malaysia*
[2]*Center for Advanced Mechanical and Green Technology, Faculty of Engineering and Technology, Multimedia University, Jalan Ayer Keroh Lama, 75450 Bukit Beruang, Melaka, Malaysia*
[3]*Department of Industrial Engineering, Faculty of Engineering and Green Technology, Universiti Tunku Abdul Rahman Kampar Campus, Jalan Universiti, Bandar Barat, 31900 Kampar, Perak, Malaysia*

Abstract. Lightweight and stiff lattice structures are good energy absorbers. This study evaluates the energy absorption capacity of a few common lattice structures printed out of PLA using fused deposition modeling and proposes an improved lattice structure. Simple cubic (SC), honeycomb (HC), body-centered cubic (BCC), and novel PeckGy80 (PG80) lattice structures were subjected to compressive tests. The quasi-static load-displacement behavior of lattice specimens was characterized in terms of specific energy absorption and crush load efficiency. The damage mechanisms were then related to energy absorption. Cracks and brittle fractures occurred in all lattice structures during the crush test. Different lattice structures induced different damage mechanisms, significantly affecting their energy absorption. SC lattice structure showed structural separation at a small displacement, rendering it an ineffective energy absorber. BCC and HC lattice structures demonstrated almost identical shear band failure modes. The PG80 lattice structure, although made of brittle PLA, displayed progressive failure from the bottom layer to the upper layers, exhibiting both a high peak load and stable post-yield behaviour. This damage mode enabled the PG80 lattice to be far superior in terms of specific energy absorption to HC, SC, and BCC lattice structures.

Keywords: 3D Printing; Energy absorption; Lattice structures; PLA; Quasi-static crush

1. Introduction

Three-dimensional lattices, having replicated structures like those of cellular solids, draw much attention owing to their high stiffness, strength and ultra-lightweight (Dong et al., 2020). Besides, the capability of lattice structures to undergo considerable deformation at a relatively low transmitted stress makes them good energy absorbers. Lightweight and large energy absorption capacity are currently the main design priorities in the automobile and aerospace sectors to minimize the amount of material and hence fuel consumption (Helou & Kara, 2017; Ye et al., 2020). Traditionally, the role of energy absorption has been filled by thin-walled tubes (Malawat et al., 2019). Recent findings indicated that polylactic acid (PLA) lattice structures might be used as sacrificial claddings as material and structure protection gear (Santos et al., 2021; Sun et al., 2021).

The advancement in additive manufacturing provides design freedom in printing

*Corresponding author's email: ckkok@mmu.edu.my, Tel.: 60-6-2523648; Fax: +60-6-2316552
doi: 10.14716/ijtech.v13i5.5829

lattices, yet the effective design strategies of complex lattices suitable for various applications are still under research (Panesar et al., 2018). Three types of lattices are common, namely strut-based lattices, planar lattices, and surface-based lattices. The typical strut-based (a.k.a. bending dominated) lattices suffer from low structural stiffness, whereas the typical surface-based (a.k.a. stretch-based) lattices demonstrate low energy absorption (Riva et al., 2021). Common strut-based lattices include simple cubic (SC) and body-centered cubic (BCC), whereas honeycomb (HC) is a common planar lattice. These common latices had been printed using different materials (Obadimu & Kourousis, 2021). In a similar study, Park and Park (2020) made functionally graded lattices, including BCC and hexagonal HC structures, with photo-curable polyurethane resin. They found that the compressive stiffness of the lattice structures varied greatly, up to five orders of magnitude depending on design parameters. And all the structures displayed predominantly bending mode in compression. Santos et al. (2021) fabricated PLA and polyethylene terephthalate glycol-modified (PETg) lattice structures out of honeycomb and auxetic-type hexagonal unit cells to investigate their low-velocity impact response. They found that PETg was superior to PLA in terms of energy absorption. A hybrid design combining an octet and a bending-dominated structure printed in PLA showed a desirable stable post-yield stress plateau, which could hardly be achieved by the octet structure alone. The latest trend also included the use of cell topology and its modification (Sun et al., 2021).

Previous work demonstrated the feasibility of SC, HC, and BCC lattices for energy absorption. Liu et al. (2021b) explored the mechanical performance of an SC lattice structure fabricated using titanium alloys through selective laser melting (SLM) technology. They found that the SC lattice structure showed manageable plateau stress and excellent energy-absorption capability, and it can be utilized in vibration damping machines and biomedical transplants (Liu et al., 2021b). It has been long observed that the HC lattice possesses a superior energy absorption ability. When loaded uniaxially, the honeycomb cells would bend and fold over steadily as demonstrated in (Ashby, 2006). On the other hand, BCC is a traditional form of bending-dominated strut-based structure, which has gained significant attention and has been experimentally and scientifically studied for its unique mechanical and energy-absorbing properties (Mines et al., 2013; Ushijima et al., 2010; Gümrük et al., 2013; Tancogne-Dejean & Mohr, 2018). The mechanical performance of the BCC lattice structure was examined under numerous loading conditions (Gümrük et al., 2013; Tancogne-Dejean & Mohr, 2018), and the classical beam hypothesis approach was used to forecast its mechanical performance (Ushijima et al., 2010; Ushijima et al., 2013). In addition, drop-weight impact tests revealed that the BCC lattice structure made of Ti–6Al–4V demonstrated superiority over the honeycomb (Mines et al., 2013), and compression tests indicated that the BCC lattice structure made of Ti–6Al–4V seemed to be suitable for energy absorption systems owing to the extended plateau region and low hardening period before densification (Tancogne-Dejean & Mohr, 2018).

Compared to other printable materials such as ABS, nylon and (PETg), PLA possesses the advantages of being biodegradable and cost-effective (Lololau et al. 2021, Santos et al. 2021). Yet, there appears to be a lack of a comprehensive evaluation of the performance of PLA-printed lattices for energy absorption, which prompted this study. There are two objectives in this study. First, the energy absorption capability of different lattice structures, namely SC, HC, BCC, and a novel PG80, was characterized experimentally to establish the basis for comparison. PG80 was not a pre-existing lattice structure but was the result of trial-and-error in the course of this work. Secondly, the structural failures of the lattice structures were related to energy absorption to elucidate the superiority of the novel lattice structure.

2. Methods

2.1. Lattice Structures and Specimen Design

The SC, BCC, and PG80 lattice structures have proper strut placement in a unit cell of 10 mm X 10 mm x 10 mm. These lattice structures, together with the HC lattice structure, have equal overall sizes of 40 mm X 40 mm X 40 mm, as shown in Fig 1. The theoretical relative density of the SC, HC, BCC, and PG80 are 0.16, 0.36, 0.26, and 0.38, respectively. The actual relative density of the printed specimens turned out to be 0.17, 0.28, 0.20, and 0.34, respectively, for the same lattice structures. The relative density is the density of the lattice structure (i.e., the mass of the lattice over its apparent volume, namely $6.4X10^4$ mm^3) over the theoretical density of the PLA, 1240 kg/m^3. To measure the actual relative density of the lattice structures, only the masses of the printed lattice structures need to be measured. The deviations in relative density may have resulted from imperfect support material removal and printing parameters. In as much as humanly possible, the printed specimens were all inspected for unintended sharp corners so that they were removed before crushing.

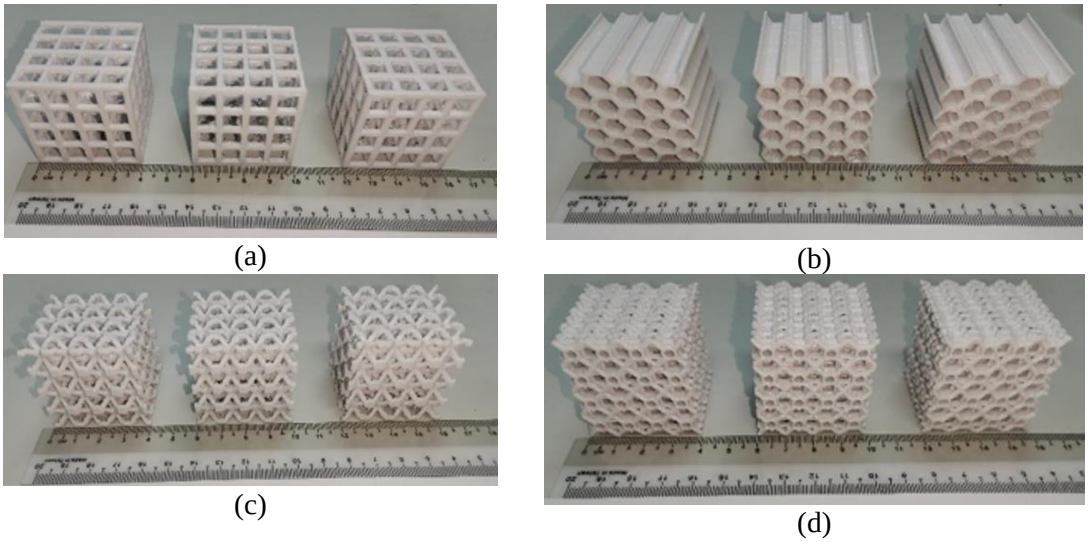

Figure 1 Printed lattice structures. (a) SC; (b) HC; (c) BCC; (d) PG80

Figure 2 shows the unit cells of SC, HC, and BCC. The SC lattice is lined with square struts having a cross-section of 2 mm X 2 mm (i.e., L = 9.5 mm and d = 1 mm in Figure 2(a)). The HC lattice was made of honeycombs in a hexagonal arrangement. Each unit cell has a perimeter of 30 mm (i.e., L = 5 mm each side, L_c = 10 mm, t = 1 mm in Figure 2(b)). When one cell is laid hexagonally with another cell, the joining side forms a honeycomb wall of 2 mm thick. The BCC lattice has eight struts per unit cell. Every strut has a cross-section of 2 mm X 2 mm, whose corners are rounded by a radius of 0.3 mm. The strut begins at the cell center and diverges to eight corners. Its length is $L \approx 7.2\ mm$ before joining a corner prism (i.e., four prisms from neighboring unit cells make a cube of 4 mm X 4 mm X 4 mm). The crossing points between trusses were made into smooth bends (see Figure 2(c)) instead of sharp corners to reduce stress concentration.

While SC, HC, and BCC lattice structures were used in this study primarily for their prevalence in previous studies, the PG80 lattice structure was designed specifically in this study to retain the existing advantage of strut-based lattice architecture, namely outstanding energy absorption, with enhancement in strength or stiffness. The PG80 unit cell comprises nodes (n) and struts (S), as shown in Figure 3. The "X" configuration nodes are generated when four struts meet at the hollow cylinder. The "#" configuration nodes are located at the struts' intersection points. The hollow cylinder that exists at the middle

of the unit cell serves as a connector that links three (3) of "X" configurations and two (2) "#" configurations in series. There are 20 struts and 20 nodes in total within a unit cell.

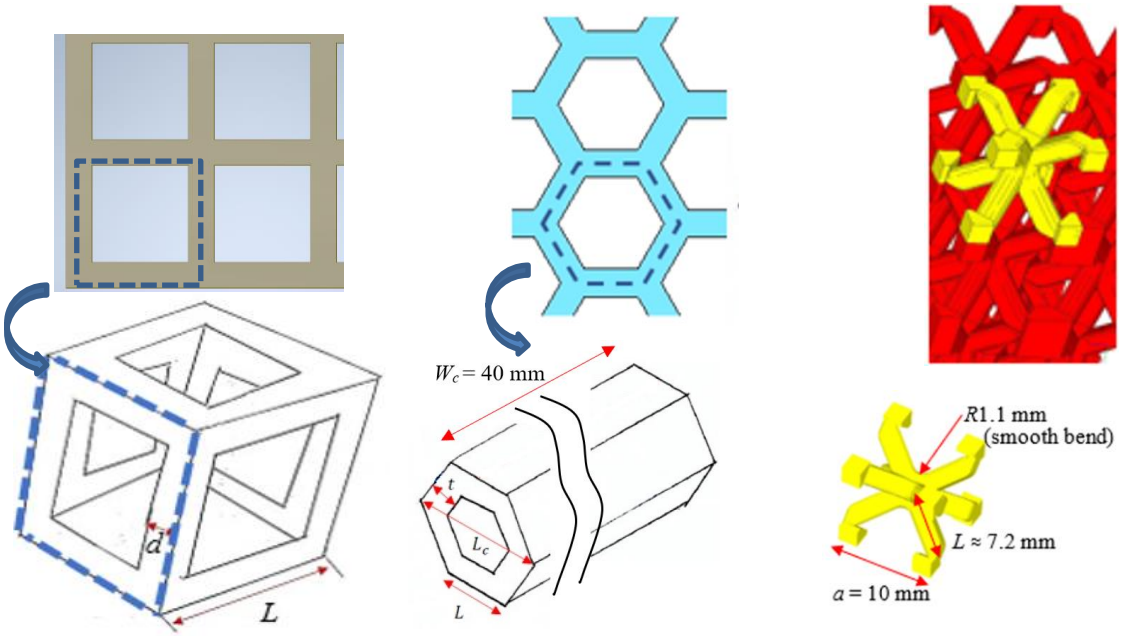

(a) (b) (c)

Figure 2 Unit cells of (a) SC, (b) HC, (c) BCC lattice structures

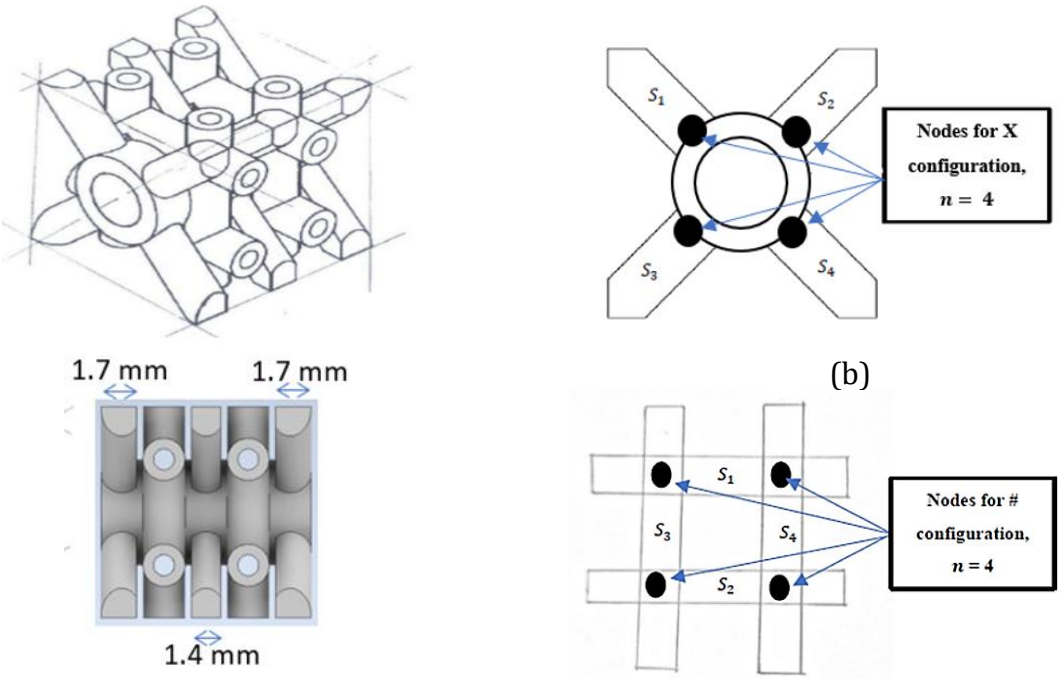

(a) (b) (c)

Figure 3 PG80 lattice; (a) Unit cell, (b) "X" configuration, (c) "#" configuration

Based on the number of nodes and struts, the Maxwell number (Maconachie, et al., 2019) turned out to be negative, making this structure exhibit a predominantly bending mode. The solid struts on the "X" have a thickness of 1.4-1.7 mm (i.e., 2 mm diameter cylinders truncated by 0.3 mm on either side and by 0.6 mm when sandwiched in the unit cell, see Figure 3 (a) (right)), whereas those hollow struts on the "#" have a mean diameter of 1.5 mm and thickness of 0.5 mm. The hollow cylinder has a mean diameter of 4 mm and is 1 mm thick.

2.2. PLA materials and printing Parameters

The lattice structures were printed out of a PLA filament with a diameter of 1.75±0.05 mm (produced by RoHS SGS (China), Brand name: LanDu). The slicing program module was used to regulate the Makerbot Replicator desktop 3D printer, which horizontally sliced the lattice structure into thin layers. The lattice structures were printed in a flat orientation, with each layer deposited in either a 0° or 90° direction, layer by layer from the bottom up. In other words, the printing direction is perpendicular to the compression direction. Printing parameters include feeding speed (3 mm/s), printing temperature (210°C), printing orientation, support building, and layer thickness. Quality was set to the default "Standard", and the layer height was set at 0.2 mm with an infill of 10%. Table 1 summarizes the typical properties of the PLA as provided by Makerbot.

Table 1 Typical PLA properties

Property	Value
Theoretical density ($\boldsymbol{kg/m^3}$)	1240
Flexural strength ($\boldsymbol{MPa}$)	61.85
Tensile strength, printed ($\boldsymbol{MPa}$)	46.77
Compressive strength, printed ($\boldsymbol{MPa}$)	17.93

2.3. Quasi-static crush Test and Energy Metrics

Universal testing machine Instron model 3367 was used to conduct quasi-static crushing of the specimens. The test speed was set at 0.5 mm/min. The machine, specimen, and compression jigs are shown in Figure 4.

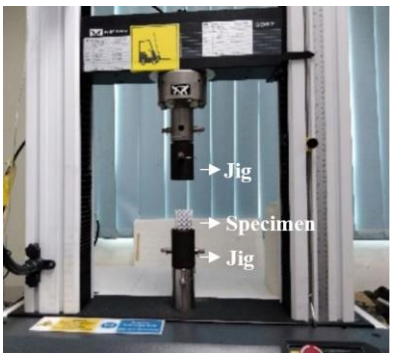

Figure 4 Photograph of compression machine, specimen, and jigs

Specific energy absorption (*SEA*) (in unit kJ/kg or J/g) and the dimensionless crush force efficiencies (*CFE*) are two metrics of particular interest in this study, as defined in Equations (1) and (2).

$$SEA = \frac{EA}{M_m} \tag{1}$$

$$CFE = \frac{F_m}{F_{max}} \tag{2}$$

where EA is the total energy absorbed (i.e., the area under the curve of the force-displacement curve before the sign of densification, in unit N-m or J), M_m is the crushed mass, F_m is the mean crush load (i.e., EA divided by crush length in unit N) and F_{max} is the maximum crush load throughout the loading history (also in unit N).

A higher specific energy absorption means a greater amount of energy absorbed per unit of mass of the crushed lattice, which indicates a more efficient absorber. Crush force efficiency is an indicator of crushing steadiness. In fact, higher crush force efficiency means lower acceleration damages (Ma et al., 2019).

3. Results and Discussion

The maximum crushing load can be acquired from the load-displacement curves in Fig 5. The curves were terminated either at the point of densification (i.e., sharp increase in load due to the compaction of crushed elements instead of structural resistance) or failure (i.e., a sudden drop in load due to structural breaking, usually visible and sometimes audible). It could be observed that SC lattice structures failed rather prematurely at small loads. HC and BCC lattice structures had lower peak loads, with HC demonstrating better energy absorption. PG80 outperformed the other three lattice structures by a wide margin in terms of the magnitude of the peak force and the stability of the post-yield behavior. The latter is favorable to energy absorption and was achieved by Sun et al. (2021) by using a hybrid lattice. The results for the samples were sufficiently consistent.

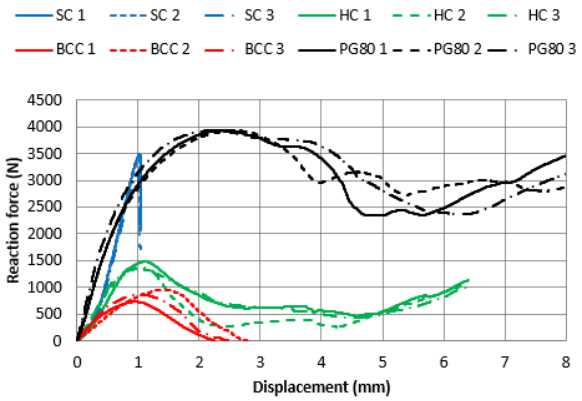

Figure 5 Load-displacement curves of different lattice structures. Specimens are designated by lattice type (e.g., SC) followed by sample number in the legend

Table 2 Energy absorption of lattice specimens

		Energy Absorption (EA), J	Specific Energy Absorption (SEA), kJ/kg	Average SEA, kJ/kg
SC	S1	1.54	0.11	0.11
	S2	1.48	0.11	
	S3	1.40	0.10	
HC	S1	4.48	0.20	0.18
	S2	3.39	0.15	
	S3	4.31	0.19	
BCC	S1	0.90	0.06	0.08
	S2	1.44	0.09	
	S3	1.17	0.08	
PG80	S1	23.47	0.87	0.87
	S2	23.76	0.87	
	S3	23.87	0.88	

Table 2 summarizes the specific energy absorption (SEA) of the samples tested for each lattice structure, where Table 3 presents the crush force efficiencies (CFE) of the same. Complying with the load-displacement curves in Figure 5, PG80 lattice structure was at least four times more efficient than the rest of the lattice structures in terms of specific energy absorption. It also demonstrated superior crush force efficiencies near 75%, while those of BCC, HC, and SC hovered around 40-55%.

Different lattice structures induced different deformation modes, which readily explained the specific energy absorption of the different lattice structures. The SC lattices failed by elastic buckling along the vertical columns and brittle fractures were visible in the

forms of "straight" clean breaks without noticeable area reduction through the cross-sections of the horizontal columns. In all the samples, a quarter of the structure completely tore off, as highlighted in the red oval in Figure 6(a) (left). The failure was catastrophic, and the structure broke into pieces (Figure 6(a) (right)). Elastic buckling and brittle failures do not favor energy absorption. Such deformation patterns were absent in Liu et al., (2021b) as the titanium alloy material they used was ductile.

Table 3 Crush force efficiencies of the lattice structures

		Max load, *N*	Mean crush load, *N*	Crush force efficiency	Average CFE
SC					
	S1	3487.50	1474.12	0.42	
	S2	3395.50	1427.33	0.42	0.42
	S3	3125.08	1348.99	0.43	
HC					
	S1	1479.45	699.59	0.47	
	S2	1361.71	529.71	0.39	0.45
	S3	1368.61	672.67	0.49	
BCC					
	S1	732.56	398.16	0.54	
	S2	951.53	514.50	0.54	0.54
	S3	862.61	472.67	0.55	
PG80					
	S1	3938.81	2933.33	0.74	
	S2	3930.73	2970.29	0.76	0.75
	S3	3929.29	2983.29	0.76	

As the force was applied beyond a threshold of around 1100 N – 1400 N in HC lattice specimens, a crushing plane appeared at the cell walls' stationary end. It then propagated along the green arrow in Figure 6(b) to the impacting end before the interim densification set in. Wall bending and brittle fractures were two common damage mechanisms. Consistent with the work of An et al. (2017), which showed "X" failure mode originating from the stationary end in their simulated aluminum honeycomb, the deflection of HC specimens in this study exhibited the "\" mode (i.e., half of the "X" mode) also originating from to the stationary end. Wall bending enhanced energy absorption and prolonged the crush period, but the brittle failure inhibited the growth of peak force.

Similar to the HC lattice, the BCC lattice structures cracked along the global direction at 45°, equivalent to some shear band (colored in beige in Figure 6(c) (left)), splitting it into two portions. The insert on the right (labeled 'x') shows a squashed crack in the band-- a brittle fracture resulting in the strut of the damaged unit cell breaking away and detaching from the node. The fracture band implied that the node encountered the highest stress at a 45 ° inclined axis. Liu et al. (2021a) observed this shear band formation in BCC and managed to suppress its formations by enlarging their aluminum alloy BCC lattice nodes. Such an approach, however, had been adopted in this study to some extent (see Figure 2(c)) and did not suppress the shear band formation.

The failure mechanism of PG80 lattice structures was totally different. The bottom layer of the structure began to fold when the displacement reached 2 mm (see Figure 6(d) (left), pink band). In particular, the hollow cylinders at the bottommost layer deformed into an irregular shape, some vertical struts buckled, and some "X" struts brittly fractured simultaneously. As the lattice structure was further compressed, similar folding

deformation propagated to the immediately upper layer of the previous fold until multiple layers failed and gradually piled up (See Figure 6(d) (right), pink band).

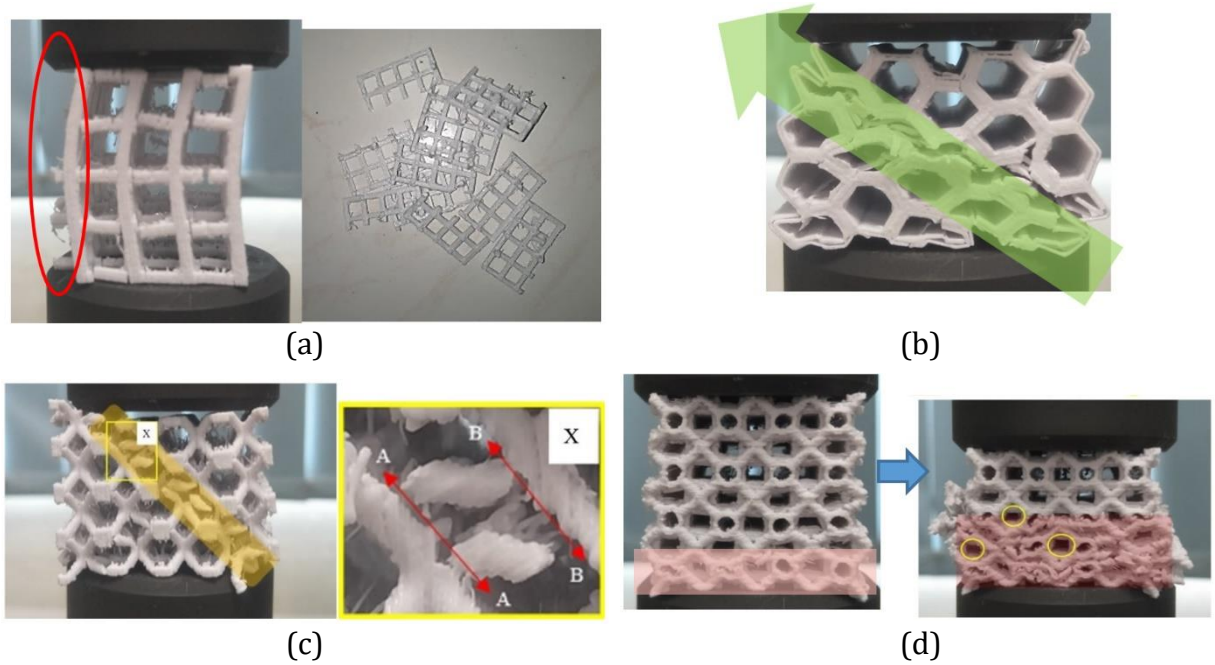

Figure 6 Deformation modes of different lattice structures. (a) SC; (b) HC; (c) BCC; (d) PG80

It is interesting to note that some ""#" configurations in a particular layer were not folded, indicating strong structural support (See Figure 6(d) (right), yellow circle). The horizontal columns of ""#" configuration were effective lacing to the vertical columns. Such ""#" configuration, when deployed in three dimensions, was shown to enhance energy absorption under compression (Ren et al., 2020). Progressive folding such as displayed in PG80 lattice, resulted in high energy absorption.

4. Conclusions

The novel lattice structure PG80 demonstrated superior energy absorption capability, at least four times greater than simple cubic, honeycomb, and body-centered cubic lattice structures. Its crush force efficiency was at 75%, which was higher than the other structures, indicating superior crush stability. SC lattice structures gave high peak force with little compression but buckled and failed catastrophically. Placing the struts diagonally towards loading in BCC lattice induced shear. Using honeycomb instead of struts in HC lattice structures induced progressive shearing. PG80's "#" configuration acted like laced columns to inhibit buckling while inheriting the high peak force of the SC lattice structure. The energy absorption of the lattice structure was closely related to the deformation modes. Buckling in SC lattice yielded the lowest energy absorption, and shear bands in BCC lattice and HC lattice absorbed crush energy slightly better. Progressive folding of printed layers from the bottom up, such as that in PG80, is much preferred for energy absorption. It is recommended that the loading directions' effect on these lattices' energy absorption be investigated to establish the superiority of PG80.

Acknowledgements

This research work has not received any grant from any funding agency. The authors are grateful to the University for granting them access to equipment to produce this work.

References

An, L., Zhang, X., Wu, H., Jiang, W., 2017. In-Plane Dynamic Crushing and Energy Absorption Capacity of Self-Similar Hierarchical Honeycombs. *Advances in Mechanical Engineering*, Volume 9(6), pp. 1–15

Ashby, M., 2006. The Properties of Foams and Lattices. *Philosophical Transactions of the Royal Society A*, Volume 364, pp. 15-30

Dong, G., Tang, Y., Li, D., Zhao, Y., 2020. Design and Optimization of Solid Lattice Hybrid Structures Fabricated by Additive Manufacturing. *Additive Manufacturing*, Volume 33, p. 101116

Gümrük, R., Mines, R., Karadeniz, S., 2013. Static Mechanical Behaviours of Stainless Steel Micro-Lattice Structures under Different Loading Conditions. *Materials Science and Engineering: A*, Volume 586, pp. 392–406

Helou, M., Kara, S., 2017. Design, Analysis and Manufacturing of Lattice Structures: An Overview. *International Journal of Computer Integrated Manufacturing*, Volume 31(3), pp. 243–261

Liu, X., Wada, T., Suzuki, A., Takata, N., Kobashi, M., Kato, M., 2021a. Understanding and Suppressing Shear Band Formation in Strut-Based Lattice Structures Manufactured by Laser Powder Bed Fusion. *Materials and Design*, Volume 199, p.109416

Liu, Y., Zhang, J., Tan, Q., Yin, Y., Li, M., Zhang, M., 2021b. Mechanical Performance of Simple Cubic Architected Titanium Alloys Fabricated Via Selective Laser Melting. *Optics & Laser Technology*, Volume 134, p. 106649

Lololau, A., Soemardi, T.P., Purnama, H., Polit, O., 2021. Composite Multiaxial Mechanics: Laminate Design Optimization of Taper-Less Wind Turbine Blades with Ramie Fiber-Reinforced Polylactic Acid. *International Journal of Technology*, Volume 12(6), pp. 1273-1287

Ma, Q., Sahat, I., Mat Rejab, M., Hassan, S., Zhang, B., Merzuki, M., 2019. The Energy-Absorbing Characteristics of Filament Wound Hybrid Carbon Fiber-Reinforced Plastic/Polylactic Acid Tubes with Different Infill Pattern Structures. *Journal of Reinforced Plastics and Composites*, Volume 38(23-24), pp. 1067–1088

Maconachie, T., Leary, M., Lozanovski, B., Zhang, X., Qian, M., Faruque, O., Brandt, M., 2019. SLM Lattice Structures: Properties, Performance, Applications and Challenges. *Materials & Design*, Volume 183, p. 108137

Malawat, M., Sumarsono, D.A., Istiyanto, J., Prayogo, G., Dionisius, F., 2019. Theoretical Prediction of Dynamic Axial Crushing on a Square Tube with Eight Holes Used as a Crush Initiator. *International Journal of Technology*, Volume 10(5), pp. 1042–1055

Mines, R., Tsopanos, S., Shen, Y., Hasan, R., Mckown, S., 2013. Drop Weight Impact Behaviour of Sandwich Panels with Metallic Micro Lattice Cores. *International Journal of Impact Engineering*, Volume 60, pp. 120–132

Obadimu, S., Kourousis, K., 2021. Compressive Behaviour of Additively Manufactured Lattice Structures: A Review. *Aerospace*, Volume 8(207), pp. 1–22

Panesar, A., Abdi, M., Hickman, D., Ashcroft, I., 2018. Strategies for Functionally Graded Lattice Structures Derived using Topology Optimisation for Additive Manufacturing. *Additive Manufacturing*, Volume 19, pp. 81–94

Park, J.-H., Park, K., 2020. Compressive Behaviour of Soft Lattice Structures and Their Application to Functional Compliance Control. *Additive Manufacturing*, Volume 33, p. 101148

Ren, H., Shen, H., Ning, J., 2020. Effect of Internal Microstructure Distribution on Quasi-Static Compression Behaviour and Energy Absorption of Hollow Truss Structures. *Material*, Volume 13(5094), pp. 1–14

Riva, L., Ginestra, P., Ceretti, E., 2021. Mechanical Characterization and Properties of Laser-Based Powder Bed–Fused Lattice Structures: A Review. *International Journal of Advanced Manufacturing Technology*, Volume 113, pp. 649–671

Santos, F., Rebelo, H., Coutinho, M., Sutherland, L., Cismasiu, C., Farina, I., Fraternali, F., 2021. Low Velocity Impact Response of 3D Printed Structures Formed by Cellular. *Composite Structures*, Volume 256, p. 113128

Sun, Z.P., Guo, Y.B., Shim, V.P.W., 2021. Characterisation and Modeling of Additively-Manufactured Polymeric Hybrid Lattice Structures for Energy Absorption. *International Journal of Mechanical Sciences*, Volume 191, p. 106101

Tancogne-Dejean, T., Mohr, D., 2018. Stiffness and Specific Energy Absorption of Additively-Manufactured Metallic BCC Metamaterials Composed Of Tapered Beams. *International Journal of Mechanical Sciences*, Volume 141, pp. 101–116

Ushijima, K., Cantwell, W., Chen, D., 2013. Prediction of the Mechanical Properties of Micro-Lattice Structures Subjected to Multi-Axial Loading. *International Journal of Mechanical Sciences*, Volume 68, pp. 47–55

Ushijima, K., Cantwell, W., Mines, R., Tsopanos, S., Smith, M., 2010. An Investigation into the Compressive Properties of Stainless Steel Micro-Lattice Structures. *Journal of Sandwich Structures & Materials*, Volume 13(3), pp. 303–329

Ye, G., Bi, H., Hu, Y., 2020. Compression behaviours of 3D printed pyramidal lattice truss composite structures. *Composite Structures*, Volume 233, p. 111706